High- and Low-Frequency Intraseasonal Variance of OLR on Annual and ENSO Timescales

DAYTON G. VINCENT

Department of Earth and Atmospheric Sciences, Purdue University, West Lafayette, Indiana

ANDREAS FINK

Institut für Geophysik und Meteorologie, Universität zu Köln, Cologne, Germany

JON M. SCHRAGE

Department of Earth and Atmospheric Sciences, Purdue University, West Lafayette, Indiana

PETER SPETH

Institut für Geophysik und Meteorologie, Universität zu Köln, Cologne, Germany

(Manuscript received 12 December 1996, in final form 11 August 1997)

ABSTRACT

Using 20 yr of outgoing longwave radiation observations, the complex behavior of the higher- (6–25-day) and lower- (25–70-day) frequency bands of tropical intraseasonal convective oscillations is investigated. Emphasis is given to the mean annual cycle and interannual variability of both bands and to the interaction between the two bands. The focus with regard to the interannual variability within each band is on the warm and cold events associated with the El Niño–Southern Oscillation (ENSO) cycle. The study encompasses the tropical and subtropical Indian and Pacific Oceans (including Australasia).

The strongest intraseasonal signals are, for the most part, aligned with the intertropical convergence zone (ITCZ) and South Pacific convergence zone. In some cases, the 6–25-day signal is not collocated with the Madden–Julian oscillation (MJO) signal and/or occurs remotely from the ITCZ. In these cases, the higher-frequency intraseasonal convective perturbations are associated with phenomena independent from the MJO, such as easterly waves, monsoon depressions, typhoons, or circulations involved in tropical–extratropical interactions. Over the equatorial eastern Indian Ocean, strong activity in both bands persists throughout the year, but the bands are found to be anticorrelated, regardless of the ENSO phase.

The effect of ENSO timescales is further examined by looking at December–February anomalies for five El Niño and two La Niña events during this 20-yr sample. A well-defined response of the two bands is restricted to the northwestern and central Pacific. Over the northwestern Pacific Ocean, the two bands complement one another with suppressed (enhanced) convection occurring during El Niño (La Niña) events. Both bands also complement each other over the equatorial central Pacific but are out-of-phase with those in the western Pacific on ENSO timescales. In contrast, over the Australian monsoon region and the eastern Indian Ocean, neither band shows a uniform response in terms of anomalous activity when the latest five ENSO warm events, 1977–78, 1982–83, 1986–87, 1991–92, and 1992–93, are considered.

1. Introduction

Intraseasonal oscillations (ISOs) of tropical convection and their associated circulation features have been the subjects of numerous papers in the published literature. Most of these papers have focused on the Madden–Julian oscillation (MJO), first proposed by Madden and Julian (1971, 1972) and recently summarized by the same authors (Madden and Julian 1994). The period of the MJO has varied among individual investigators, but it usually lies within the range of 25–70 days. By comparison, a smaller number of papers has addressed the higher-frequency band of ISOs, which generally falls within the period of 6–25 days. It is the latter band, therefore, which represents the main interest in the present investigation. However, the convective oscillations within both bands are examined so that their relative importance can be compared and contrasted.

The primary purpose of this study is to provide a comprehensive documentation (climatology) of the an-

Corresponding author address: Dr. Dayton G. Vincent, Department of Earth and Atmospheric Sciences, Purdue University, 1397 Civil Engineering Building, West Lafayette, IN 47907-1397.
E-mail: dvincent@meteor.eas.purdue.edu

nual and interannual variability of convective activity associated with the ISOs within the two bands noted above. Our focus will be on the extent to which the interannual variability in both bands varies systematically with the phase of the El Niño–Southern Oscillation (ENSO). In this regard, almost no attention has been devoted to the interannual variability of convection on 6–25-day timescales. The traditional seasons of (December–February) (DJF), March–May (MAM), July–August (JJA), and September–November (SON) will be used to examine the annual cycle, and 20 yr of outgoing longwave radiation (OLR) data (1974–1994) will be applied to investigate interannual variability. During this time span, five El Niños and two La Niñas occurred.

In order to provide the background for our study, summaries of the MJO (25–70-day band) and 6–25-day band ISOs are given in section 2. A discussion of data sources and computational procedures is presented in section 3. Section 4 provides a discussion of the seasonal climatologies and annual variability of the ISO convection bands. Section 5 contains results of the interannual variability within our two convective bands, while section 6 discusses the correlations between the two bands. Finally, some concluding remarks are given in section 7.

2. Summary of important features of ISO bands

a. MJO

As mentioned in the introduction, numerous papers have been written concerning the MJO; therefore, only a few of the papers most relevant to our study are cited. Wang and Rui (1990) provide an excellent climatology of transient tropical intraseasonal convection anomalies for the period 1975–85 based on OLR data. They identified 122 convective events, of which 77 were classified as eastward propagating and within the MJO range. Wang and Rui (1990), as well as Rui and Wang (1990), found that the MJO was strongest (i.e., coldest cloud tops) at 0°, 82°E, with a broad secondary maximum of convection in this band at the equator between 120° and 150°E. These authors note that MJO events became nearly stationary in the central Indian Ocean, which is the region of highest occurrence and maximum intensification. Several investigators, including the original authors (Madden and Julian 1972), have noted that the convective signal of the MJO usually dissipates near the dateline, even though the upper-level divergence signal propagates around the globe. Other authors have suggested that a dipole or seesaw pattern between the central Indian and western Pacific Oceans occurs as the MJO convective events propagate eastward (e.g., Lau and Chan 1985; Weickmann et al. 1985; Zhu and Wang 1993).

Two of the more relevant discussions related to the interannual variability part of our investigation are given by Gutzler (1991) and Anyamba and Weare (1995).

Gutzler found that the variance in MJO lower-tropospheric winds was enhanced during ENSO warm events but only over the Pacific Ocean for stations between 140°E and 170°W. He found no identifiable interannual behavior of these winds west of 140°E. Anyamba and Weare noted that a marked variability occurred in the MJO's spatial characteristics for the El Niños of 1976–77, 1982–83, and 1986–87.

Before moving on to a summary of 6–25-day ISOs, it is important to note that the western Pacific MJO convective events typically are composed of a hierarchy of organized cloud clusters, which occur on smaller space and shorter timescales than the MJO. It has been well documented that, when the convection associated with an MJO is reenhanced as it reaches the western Pacific, it often consists of a large-scale envelope of convection, which contains eastward-propagating super cloud clusters (SCCs), as well as westward-propagating cloud clusters (CCs) (Nakazawa 1988; Lau et al. 1989; Lau et al. 1991; Sui and Lau 1992). The temporal scale of SCCs is 1–2 weeks, thus the large-scale envelope of convection mentioned above provides an example of scale interaction between our two ISO bands.

b. The 6–25-day band

As noted in the introduction, the attention devoted to this band in the literature is much less than that which has been devoted to the MJO. For this reason, we are able to provide a nearly comprehensive review of the 6–25-day band. This band contains several physical phenomena, which include, but are not restricted to, super cloud clusters, monsoon depressions, tropical cyclones, Rossby wave trains, dipoles of convective activity in the zonal and meridional planes, and subtropical jet streaks. In general, as one proceeds from the equator (or perhaps the thermal equator) toward midlatitudes, the occurrence (or recurrence) of convective phenomena on 6–25-day timescales increases.

The main part of our review will focus on summaries of four papers (Kiladis and Weickmann 1992a,b; Kiladis et al. 1994; Meehl et al. 1996), which we found to be the most relevant to establishing the background and purpose of our paper. The Kiladis et al. paper acknowledges that little work has been done on the 6–30-day ISO band, and the authors state that convective activity within this band is very important, particularly over the western Pacific in northern winter. They further state that the use of "the rather broadband 6–30-day filter effectively removes most variability associated with the MJO, with the 6-day cutoff eliminating the bulk of the variability due to westward propagating Rossby-gravity modes and synoptic-scale baroclinic processes outside the Tropics, as well as noise due to erroneous data assimilation." We concur with this statement, and it is one of the reasons why we selected 6–25-day bandpass filtering. Kiladis et al. examined convective events on 6–30-day timescales for 6 yr during the November–Feb-

TABLE 1. Selected list of references that focus on spectral peaks of convection and related variables in the 6–25-day band for six regions across the Indian and Pacific Oceans.

Region	References	Variables	Season	Spectral peaks (days)
Southwest Indian Ocean	Jury and Pathack 1991	Kinematic	SH summer	7–28
	Jury et al. 1991	Satellite imagery	SH summer	10–20
Bay of Bengal, India	Nitta et al. 1985	OLR, kinematic	NH summer	6
	Hartmann and Michelsen 1989	Precipitation, kinematic	NH summer–fall	5–9, 15
	Lau and Lau 1990	OLR, kinematic, thermo-dynamic	NH summer	7–8, 15
Northwest Pacific	Nitta and Takabayu 1985	Kinematic	NH summer–fall	6–10
	Lau and Lau 1990	OLR, kinematic, thermo-dynamic	NH summer	7–8
	Hartmann et al. 1992	Kinematic	NH fall	20–25
	Schnadt 1997	OLR, kinematic, thermo-dynamic	NH fall–early winter	6–25
SH Western Pacific	Vincent et al. 1991	OLR	SH summer	10–25
	Ko and Vincent 1996	Kinematic	SH summer	5–20
	Vincent et al. 1997	OLR, kinematic	SH summer	7–14
SH ITCZ, SPCZ	Vincent et al. 1991	OLR	SH summer	8–20
	Kiladis and Weickmann 1992a	OLR, kinematic	SH summer	15–25
	Schrage and Vincent 1996	OLR, kinematic	All year	7–21
NH Eastern Pacific, ITCZ	Lau and Lau 1990	OLR, kinematic, thermo-dynamic	NH summer	3–8
	Kiladis and Weickmann 1992b	OLR, kinematic	NH winter	6–14
	Fuell 1997	OLR	NH summer–fall	7–25

ruary season, beginning with 1986–87 and compared their results with MJO convective events. They found that tropical–extratropical interactions were an important part of the role played by 6–30-day oscillations in winter over the Northern Hemisphere (NH) region stretching from the central Indian Ocean to the western Pacific.

Meehl et al. (1996) conducted a follow-up study to their earlier paper (Kiladis et al. 1994; the first three authors are the same) and further documented the relationships between convective events on MJO and 6–30-day timescales during northern winter. They found that convection over the Indian Ocean, which occurred on both timescales but was contained within an MJO envelope, was linked to convection on the 6–30-day timescale over the NH eastern Pacific ITCZ. This link was manifested through upper-tropospheric wave trains that were from the Tropics to midlatitudes and back to the Tropics. They noted that a similar pattern existed in the Southern Hemisphere (SH), but it was much weaker than its NH counterpart.

A scenario similar to that described by Meehl et al. (1996) was also suggested by Kiladis and Weickmann (1992b), who found that Rossby-type wave trains enhanced convection anomalies on 6–14-day timescales during the winter season in the NH eastern Pacific ITCZ. They also found that the *subtropical* portion of the SPCZ had convective flareups on 14–30-day timescales due to wave trains in the SH; however, Kiladis and Weickmann (1992a) showed that the *tropical* portion of the SPCZ did not contain significant convection on either the 6–14-day or 14–30-day timescales.

To complete our review, we refer to Table 1, which provides a convenient summary, according to geographical location, of most of the work published (that has not already been referenced) on ISOs in the 6–25-day band. A few highlights from some of the papers are now given at each of the six geographical regions. Jury et al. (1991) used 15 yr of data (1970–84) to examine convective disturbances and tropical cyclones over the southwestern Indian Ocean between 10° and 20°S. They found that approximately one-half of the years contained westward-propagating disturbances, while most of the remaining years were dominated by quasi-stationary systems. They also found that there were more convectively active systems during the years containing westward-propagating disturbances. In the Bay of Bengal–India region, Nitta et al. (1985) attributed the 6-day signal they found over the northern Bay of Bengal to westward-propagating depressions along the monsoon trough over northeastern India. Hartmann and Michelsen (1989) used 70 yr (1901–70) of precipitation data and found significant spectral peaks from 5–9 days along the east coast of India. These peaks were associated with the northwestward tracks of monsoon lows.

Over the northwestern Pacific region, Nitta and Takabayu (1985) suggested that the 6–10-day spectral peak they found in OLR during summer and fall was caused by west-northwestward-propagating disturbances that frequently developed into tropical cyclones and typhoons as they tracked from about 10°N, 170°E toward Taiwan. Hartmann et al. (1992) used rawinsonde data to infer that a spectral peak they found in the 20–25-day band during the 4-month period, September–De-

cember, was related to typhoon activity. This peak was significant between the equator and 15°N and stretched westward from 170°W to 120°E. Schnadt (1997) used 10 yr (1985–94) of OLR data to examine the importance of 6–25-day variability on tropical–extratropical interactions over the northwestern Pacific. Her study focused on tropical cyclone activity during the fall and early winter season. She found that the axes of minimum OLR, maximum variance of OLR in the 6–25-day band, and the mean track of nonrecurving tropical cyclones (Frank 1985) were nearly coincident. Schnadt also examined recurring cyclones and found a tongue of high 6–25-day variance aligned with their mean track. Finally, she found that all of her ensemble energy spectra of OLR for September–December, 1985–94, exhibited statistically significant peaks at 6–10 days and 15–18 days over the region bounded by 10°–15°N, 130°–145°E. The former peak is identical to that found by Nitta and Takabayu (1985); however, the latter peak is believed to be a new finding.

The next two regions given in Table 1 are adjoining, and sometimes the processes and phenomena in one region affect or interact with those in the other. In the SH western Pacific, Vincent et al. (1997) looked at 4 yr (1985–89) of OLR and wind data for the 6-month summer season, November–April. They found that, in at least 50% of the 40 cases they examined, tropical forcing through a local Hadley-type circulation was responsible for the observed accelerations in subtropical jet streaks, which propagated eastward from eastern Australia toward the central Pacific. Since these jets recur on 1–2-week intervals, they speculated that the tropical heat source, which was responsible for the forcing, was active within the 6–25-day band. Their results point to another example where oscillations on 6–25-day timescales might be responsible for tropical–extratropical interactions. In the adjoining SH–ITCZ–SPCZ region, Schrage and Vincent (1996) used 6 yr (1985–90) of OLR and upper-air analyses to document 29 episodes of large-scale circulation patterns that were dominated by repeated cycles of 7–21-day convective variability, each lasting up to about 4 months. They also found that a dipole existed in their patterns, in that when convection was active in the equatorial western Pacific (ITCZ), it was inactive in the subtropical central South Pacific (SPCZ) and vice versa. Their results, therefore, show still another example of tropical–extratropical interactions within the 6–25-day band.

Finally, for the NH eastern Pacific-ITCZ region, we will cite some recently completed research by Fuell (1997). He used 15 yr (1979–94) of OLR data and computed total variance (with the annual cycle removed) and variance associated with 3–7- and 7–25-day bandpasses for four periods: two 4-month seasons, December–March (DJFM) and July–September (JJAS); and two 2-month transition seasons, April–May (AM) and October–November (ON). In JJAS, and to a certain extent also in AM and ON, he found that the axes of

minimum OLR (ITCZ) and maximum variance of 3–7-day bandpass-filtered OLR were essentially coincident along about 10°N. Presumably, this is due to westward-propagating waves. More important to this paper, however, is his result that the axes of maximum total and 7–25-day variance generally coincide, but are not always coincident, with the ITCZ. In particular, the axes of both maxima meander to a location about 5° north of the ITCZ between approximately 125° and 90°W in AM, JJAS, and ON. He speculates that this is due, in part, to tropical cyclones that have developed and moved away from the ITCZ. It could also be partly due to enhanced convection on 6–14-day timescales that emanate from Rossby-type wave trains, as proposed by Kiladis and Weickmann (1992b).

3. Data sources and computational procedures

Since one of the primary goals of this paper is to document the ENSO variability of the ISO bands, the length of the dataset is of prime importance. The investigation period will be 20 yr, from July 1974 to April 1994, as dictated by the advent of operational measurement of OLR by NOAA polar-orbiting satellites. These OLR data are provided as twice-daily means at increments of $2.5° \times 2.5°$ lat–long for the entire period, except for 9 months in 1978 when they were missing. Gruber and Krueger (1984) state that, at the time of their paper, inhomogeneities due to changes in satellite instrumentation had been corrected, and the use of twice-daily means minimizes the effect of different equator crossing times. Values of the Southern Oscillation index (SOI) will be used here to provide a measure of the phase of ENSO. They are based on 5-month running means given by the Climate Analysis Center (CAC). The CAC SOI is computed as the normalized difference of the monthly mean sea level pressure anomalies between Darwin and Tahiti.

To quantitatively assess the strength of the convective signals in each band, we utilized the variance of bandpass-filtered OLR over each of the 74 3-month seasons DJF, MAM, JJA, and SON. For each 91-day season, the variance is defined as

$$\sigma^2_{(\text{band})(\text{season})} = \sum_{n=1}^{91} \frac{[\text{OLR}_{\text{band}}(n)]^2}{90}. \quad (1)$$

The subscript band is added to (1) to emphasize that the 6–25- and 25–70-day bandpass-filtered OLR data enter the formula. Anomalous seasonal activity in either band is assessed by subtracting the long-term seasonal mean from the seasonal value [denoted by the overbar in (2)]; that is,

$$(\sigma^2_{(\text{band})(\text{season})})' = \sigma^2_{(\text{band})(\text{season})} - \overline{\sigma^2_{(\text{band})(\text{season})}}. \quad (2)$$

Thus, the seasonal anomalies in this paper not only contain variations with periods longer than 1 yr, but also intraannual perturbations from the normal annual cycle with periods between 3 months and 1 yr. Our approach
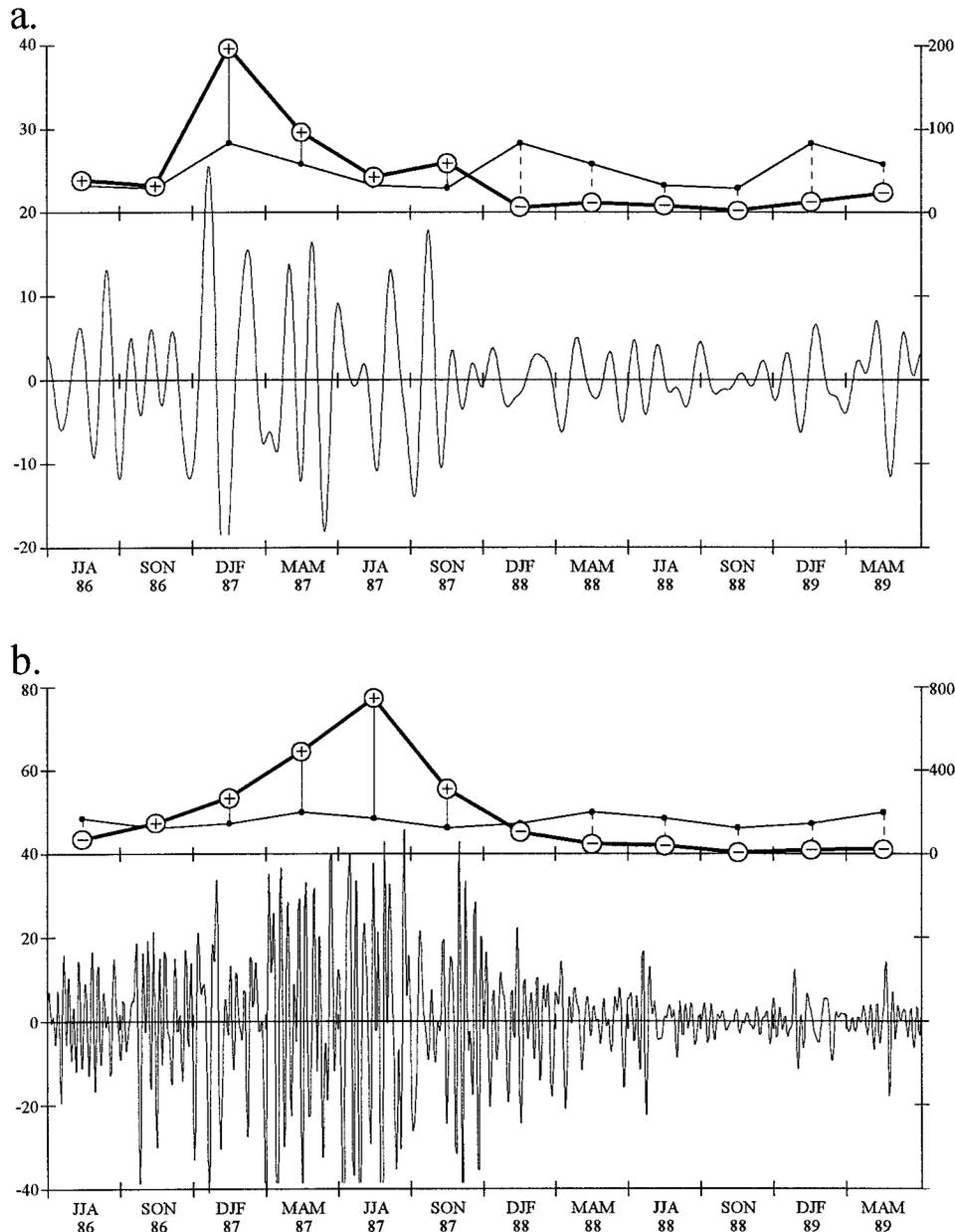
FIG. 1. A demonstration of how seasonal variance anomalies are computed from (a) 25–70-day and (b) 6–25-day bandpass-filtered daily OLR data. The series shown are from June 1986 through May 1989 at 0°, 160°W (units are W m^{-2}, using the left axis). The thick curve represents the variance of the filtered data within each season (units are W^2 m^{-4}, using the right axis). A repeating cycle of the ''mean'' seasonal variance is also depicted, with anomalies from this mean pattern suggested by + and − symbols on the thick line.

to assess interannual variance anomalies in a given frequency band is almost identical to the one described in Murakami and Sumathipala (1989) except that they used the Murakami filter. Gutzler (1991) and Schrage and Vincent (1996) also used similar surrogate variables to investigate anomalies of intraseasonal convective oscillations in the lower- and higher-frequency bands, respectively.

In order to illustrate the variance measures given in (1) and (2), their evolution during the complete ENSO cycle between JJA 1986 and MAM 1989 is displayed in Fig. 1 for a grid point in the equatorial central Pacific. As is evident from the bandpass-filtered daily OLR data (Figs. 1a and 1b, lower curves), the amplitudes of the 6–25- and 25–70-day oscillations vary between the 1986–87 El Niño and the 1988–89 La Niña by as much
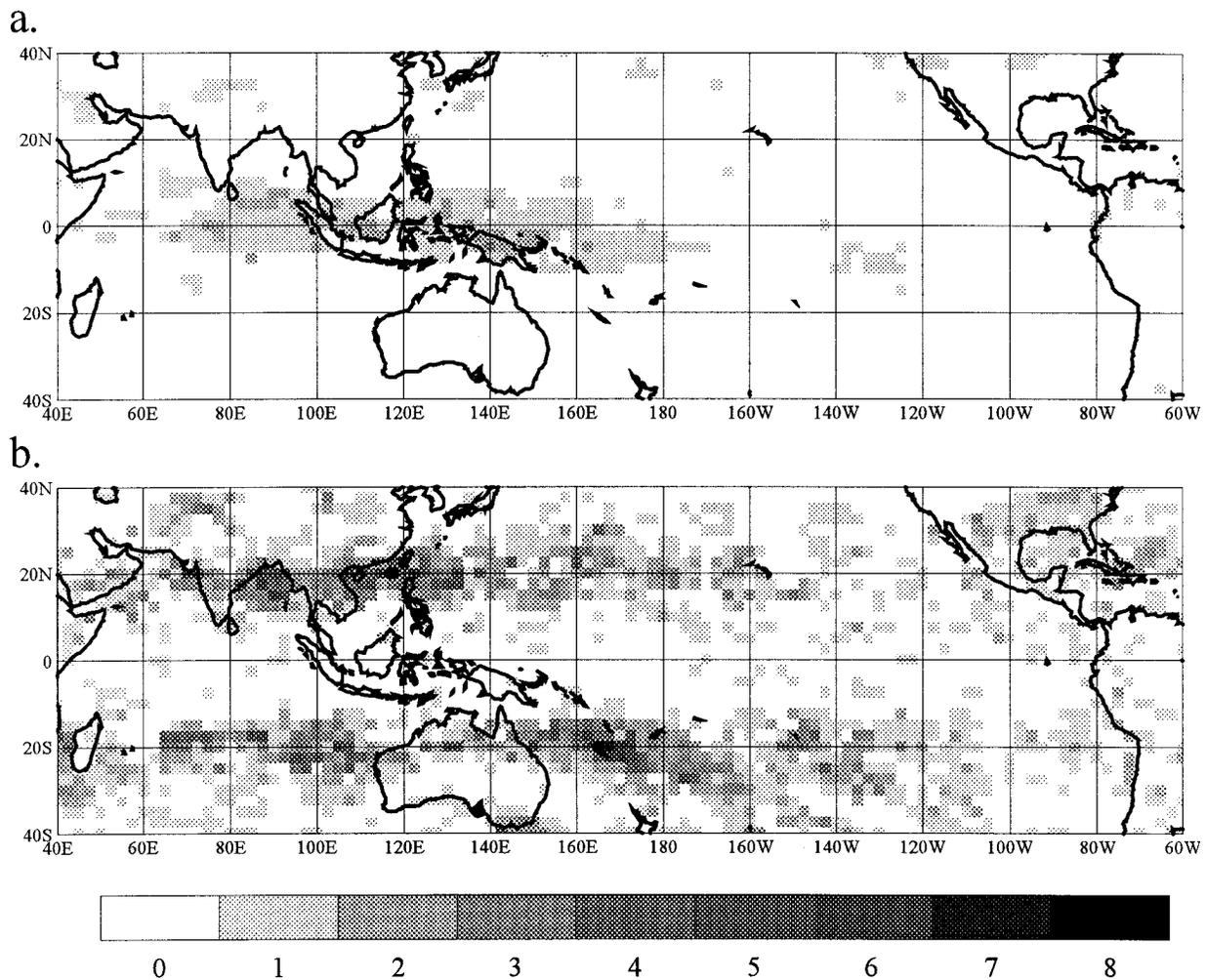
a.

b.

FIG. 2. Number of frequencies with power greater than the 99% confidence threshold in the (a) 25–70-day and (b) 6–25-day band, based on an ensemble FFT of 43 128-day time series of OLR between 1979 and 1994 at each grid point. There were 4 (16) frequencies in the 25–70- (6–25-) day band; therefore, the binomial distribution suggests that any given grid point's time series has a probability of approximately 0.04 (0.15) of containing at least one significant frequency by pure chance.

as a factor of 4. Spectra obtained from the maximum entropy spectral analysis method (not shown) indicated highly significant spectral peaks in both bands for the March–August period in 1987, whereas the spectrum for the respective time span in 1988 did not show significant peaks in either intraseasonal band. As a consequence of the oscillations' amplitudes being modulated by the phase of ENSO, the seasonal variances are well above the long-term seasonal mean during El Niño 1986–87 and drop to below normal values during the subsequent 1988–89 La Niña event. The actual $\sigma^{2\prime}$ values (i.e., the differences between the seasonal variance and the long-term seasonal mean) are suggested by the vertical lines, as are the signs of anomalies by the + and − symbols on the thick curve. In the example shown in Fig. 1, the σ^2 time series reasonably mimic the change from seasons that have intraseasonal convective signals to seasons where no signals are present due to the ab-

sence of deep convection. It is worth noting that, even in areas where deep convection is present all year around (e.g., over the warm pools), the variations of $\sigma^{2\prime}$ reflect both modulations of the oscillations' amplitude and the duration of "nonsignal" episodes.

To assess the overall significance of the bands, maps have been produced that show the number of frequencies in either band, which exceeds the 99% confidence threshold of an ensemble FFT for 43 128-day time series of OLR between 1979 and 1994. As was expected, significant peaks in the MJO band are confined to a 20° latitudinal belt straddling the equator from the central Indian Ocean to the dateline (Fig. 2a). In contrast, significant signals in the 6–25-day band are quite well aligned with the 20th parallels in either hemisphere (Fig. 2b). As mentioned earlier, the higher number of significant frequencies in the 6–25-day map is due to the fact that this frequency contains four times more frequencies
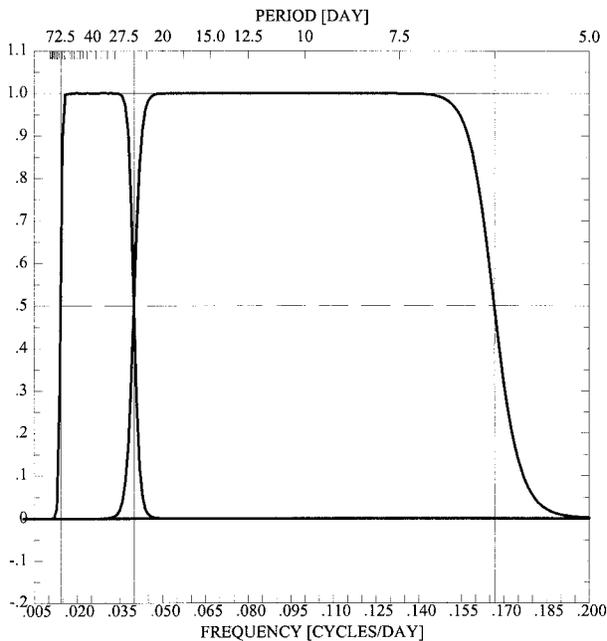
Fig. 3. Frequency response functions for the 6–25- and 25–70-day Butterworth bandpass filters.

than the MJO band. The number of significant frequencies within the band is not intended to suggest either the number of important spectral peaks or the width of the significant band; rather it is an expression of our confidence that spectral peaks exist in the given band. However, it cannot be inferred from Fig. 2b that the off-equatorial signals represent convective oscillations rather than cirrus cloud signals associated with the subtropical jet streams. Current knowledge (cf. section 2b), as well as the corresponding seasonal maps suggest that, over the following areas, the signal is mainly due to convective oscillations in the respective summer seasons: the northern Bay of Bengal and the northern parts of the South China and Philippine Seas, and the SH subtropical western Indian and Pacific Oceans in northern winter.

The filtering of the daily OLR data was performed using a 20th-order, computationally efficient recursive Butterworth bandpass filter (Stearns and Hush 1990). Its frequency response functions for the 6–25- and 25–70-day period interval are shown in Fig. 3. In contrast to the widely used recursive Murakami bandpass (Murakami 1979), which has a peak response of 1.0 only near the center of each band, the high-order Butterworth filter applied here approximates a step function and does not attenuate a spectral peak located in either of the broad passbands. Obtaining both a full response in as broad a spectral band as possible within a given interval and a minimum overlap of the bands is an appropriate approach for two reasons: 1) The signals investigated here are characterized by a high variability in the location of their peak frequencies, and 2) the chances that

a strong signal with a period close to 25 days contributes to anomalous power in both bands solely due to a non-optimal filter choice are minimized. There is, however, a trade-off between the steepness of the filter and the data lost at the beginning and end of a time series. One (two) month(s) has (have) been omitted at either end of the 6–25- (25–70-) day filtered time series. Thus, a total of 74 seasons were available between SON 1974 and DJF 1993–94, with MAM 1978–DJF 1978/79 missing.

4. Annual cycle of ISO convection bands

This section contains a discussion of the seasonal changes of the bandpass-filtered variance on 25–70- and 6–25-day timescales. As is frequently done, we assume that OLR variance is representative of the variability in convective activity, an assumption that should be valid for most of the low-latitude regions examined in this study (see section 3). The 20-yr mean OLR patterns for each 3-month season were computed but are not shown because they are very similar to those produced by other authors who used a subset of our period (e.g., Meehl 1987 for the 8 yr 1974–77 and 1979–83; Vincent and Schrage 1995 for the yr 1985–90; and Murakami 1980 for three DJF seasons only).

a. Seasonal changes in the 25–70-day bandpass variance of OLR

Figure 4 shows the seasonal changes in the 25–70-day bandpass-filtered variance of OLR. Shading represents the percent variance explained (%VE) by the 25–70-day band computed with respect to the total variance of OLR with the annual cycle removed. Figure 4 reveals that peak values of variance occur over the central Indian Ocean during all four seasons, with only minor seasonal changes. In this region, the %VE by the 25–70-day convective band is generally greater than 25% and is greater than 30% in MAM and JJA. This verifies the earlier findings described in section 2a regarding the importance of the MJO in causing and maintaining convection over the Indian Ocean. In contrast, Fig. 4 shows that a region with persistently low MJO variance, as well as %VE, is the Maritime Continent with local minima over the big islands. This also agrees with the findings of several scientists who noted that the importance of MJO convection appears to diminish over the Maritime Continent relative to other convective timescales. It is interesting, however, that the pattern of low power and %VE seems not to hold over northern Australia in DJF.

The most striking feature in Fig. 4, with regard to seasonal differences in the patterns of variance and %VE, is the contrast between the patterns of DJF and the other three seasons. The SH Tropics show that the axes of maximum variance, minimum OLR (see dotted line on Fig. 4), and maximum %VE are nearly aligned along 5°–10°S from the eastern Indian Ocean to the
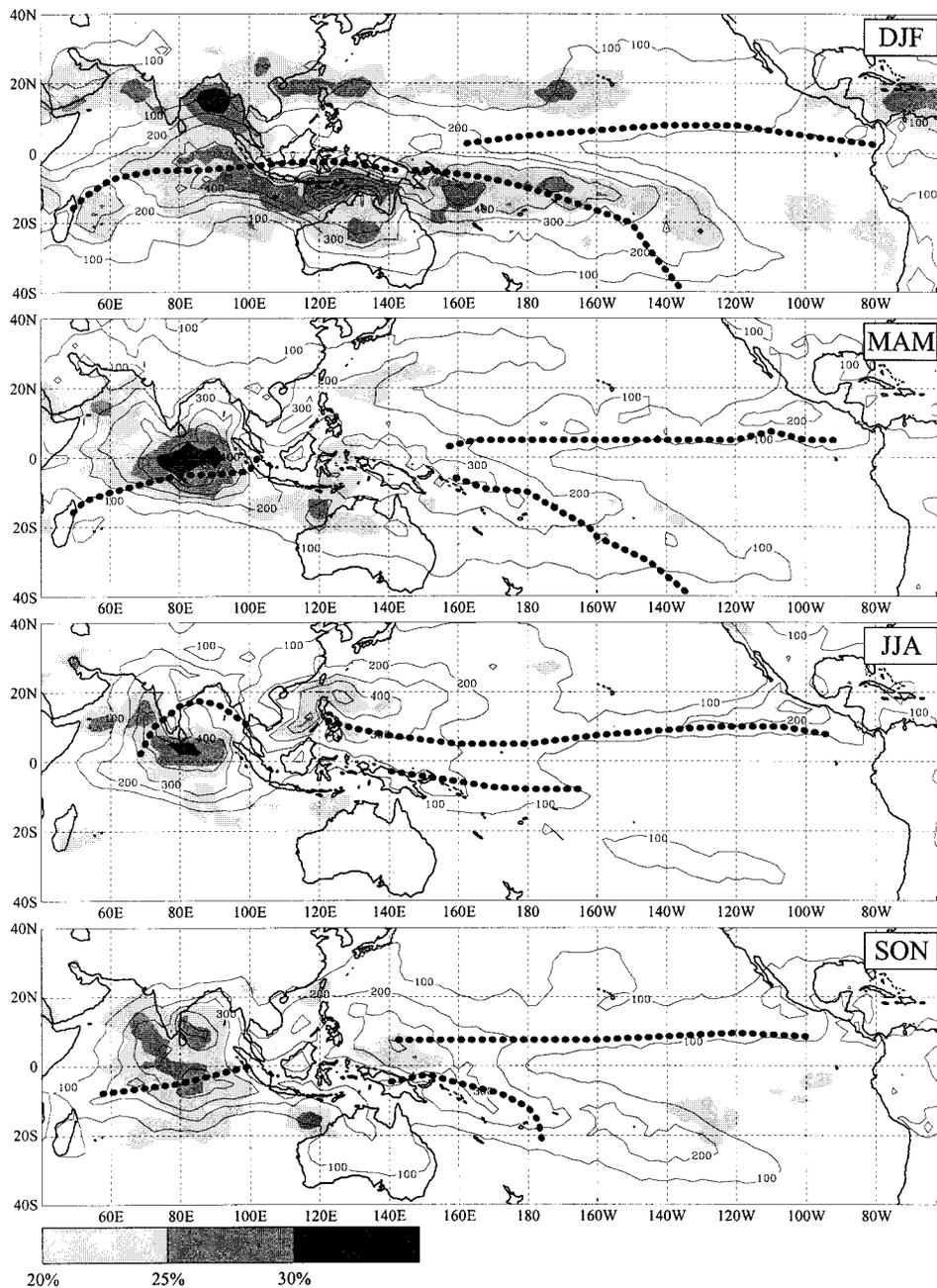
FIG. 4. Variance of 25–70-day bandpass-filtered OLR in $W^2 \, m^{-4}$, for the seasons indicated. Shading represents the percent of the total variance (with the annual cycle of OLR removed) explained by the 25–70-day band. Dotted lines represent the axes of minimum OLR.

central Pacific Ocean. The NH shows an expansive belt along 20°N, from 40°E (edge of the map) to the central Pacific, where the %VE by the 25–70-day band exceeds 20%. Although this is an interesting feature, it most likely is not associated with deep convection, since this belt contained high values of OLR (not shown).

There are four regions worth noting where large seasonal changes in MJO variance occur. The first is over the northern Bay of Bengal, where low values occur in

DJF, but much higher values exist for the remaining three seasons. MJO activity is an important aspect of this monsoon season. The second region is over northern Australia and its adjacent coastal areas, where high values are present in DJF but not in the other three seasons. This region had the highest maximum of total OLR variance in DJF (not shown), and Fig. 4a shows that the MJO plays an important role in the total convective variability there. That is, at least 25% of the total vari-

ance is explained by the MJO in much of this region. In this regard, it has been demonstrated that an MJO convective event generally initiates the Australian monsoon in the summer season (e.g., Hendon and Liebmann 1990). The third region where large seasonal fluctuations occur in the 25–70-day OLR variance is the NH South China and Philippine Seas. In that region, maximum variance coincides with high values (>20%) of %VE during JJA, but both features decrease substantially in the remaining seasons. The SPCZ represents the fourth region, which exhibits large seasonal changes in MJO variance. In DJF, the axis of maximum variance is well aligned with values of %VE greater than 20% over a considerable area, whereas in the other three seasons, the MJO band does not seem to be important.

For comparison with our results, one of the appropriate references is Lau and Chan (1988), who used data from 1974 to 1986 to compute intraseasonal variance for two 6-month periods. Their winter and summer periods showed the same patterns as our MJO bands for DJF and JJA, respectively, but their values were considerably smaller than ours over most of the analysis region. The most plausible explanations for this difference are 1) they used a 5° × 5° lat–long grid, whereas we used a 2.5° × 2.5° grid; 2) they averaged over 6 months, while we averaged over 3 months; and 3) their filter has a different response function than ours. As another example for comparison, we cite the results of two related papers by Weickmann et al. (1985) and Knutson et al. (1986). They used 10 yr of OLR data and also averaged over two 6-month periods, with the former (latter) paper examining the northern winter (summer) period. As for Lau and Chan, their results were very similar to ours, but their peak values were greater than those given by Lau and Chan and less than ours. It should also be noted that our axes of maximum variability generally correspond to the preferred tracks of MJO events given by Wang and Rui (1990).

b. Seasonal changes in the 6–25-day bandpass variance of OLR

The seasonal changes of the 6–25-day band variance of OLR are illustrated in Fig. 5. As for Fig. 4, the axes of minimum total OLR and %VE by the band are also shown. Note that the shading for %VE is different from that in Fig. 4. Of course, the frequency domain occupied by the 6–25-day band is broader than that within the 25–70-day band (Fig. 3). Keeping this in mind, the foremost feature in Fig. 5 is that values of variance are about twice as large as they were in the MJO band. As for the 25–70-day band, seasonal changes in the 6–25-day band over the equatorial central Indian Ocean are only slight. Maximum variability in that region is centered over the SH Tropics in DJF. In MAM, maximum variability moves to the equator and then increases slightly in the NH Tropics in JJA, with peak values located in the Bay of Bengal. Over the latter region, the %VE

reaches an extremely high value of 50% for the 6–25-day band in JJA. It would appear that wave disturbances and tropical cyclones on timescales of 6–9 days are responsible for much of this variance (e.g., Nitta et al. 1985; Hartmann and Michelsen 1989; and Lau and Lau 1990). In SON, the 6–25-day variance in the Bay area decreases slightly, as does the %VE, but both remain quite high. The explained variance by the MJO band was also quite large over the Bay of Bengal in SON.

Several other regions show an appreciable annual cycle in the 6–25-day convective band. In the SH, the SPCZ contains high values of variance in DJF but lower values in JJA. The JJA maximum, poleward of 20°S, is a manifestation of intruding baroclinic systems (Schrage and Vincent 1996) rather than a direct influence of tropical convection. This effect may be responsible for the general poleward displacement of the axis of 6–25-day variability relative to the 25–70-day axis during all seasons in the South Pacific (compare Figs. 4 and 5). The large values of variability in DJF, which are also evident in MAM and SON, appear to be influenced by subtropical jet streaks, which propagate eastward across the SH western Pacific with a quasi-regular period of 1–2 weeks from early November until mid-April (e.g., Ko and Vincent 1995, 1996). Figure 5 shows that the %VE by the 6–25-day convective band in the SPCZ is substantial, especially in the subtropics. Large areas in excess of 45% occur in all seasons. This result agrees with Meehl et al. (1996) and others. There is also a region of maximum variance in the 6–25-day band over northern Australia in DJF, which is much weaker in the other three seasons. Recall that a maximum in the MJO band occurred in the same season along the northern coast of Australia. In contrast to the MJO band, however, the 6–25-day band over northern Australia does not show a high percentage of variance explained in DJF.

In the NH, there are two regions that exhibit high seasonal variability in the 6–25-day band. One is located in the western Pacific along the northern edge of the warm pool area, where peak values occur near 15°N in JJA. These values decrease slightly in SON and are much smaller in the subsequent two seasons. This region also contained maximum variance in JJA and SON in the MJO band. Note that the axis of maximum variability is more zonally oriented in JJA and more diagonal in SON. This phenomenon, which is related to the track and frequency of westward-propagating tropical disturbances and typhoons in both seasons, has also been studied by Nitta and Takabayu (1985). The other region, which shows notable seasonal changes in the NH, is the area near the eastern Pacific ITCZ. As for the western Pacific, the maximum variance occurs in JJA and persists into the SON. The percent variance explained by the 6–25-day band in the eastern Pacific is also quite large, both in JJA and SON, and has been related to the higher frequency portion of this band (i.e., 6–8 days) by Lau and Lau (1990) and others.
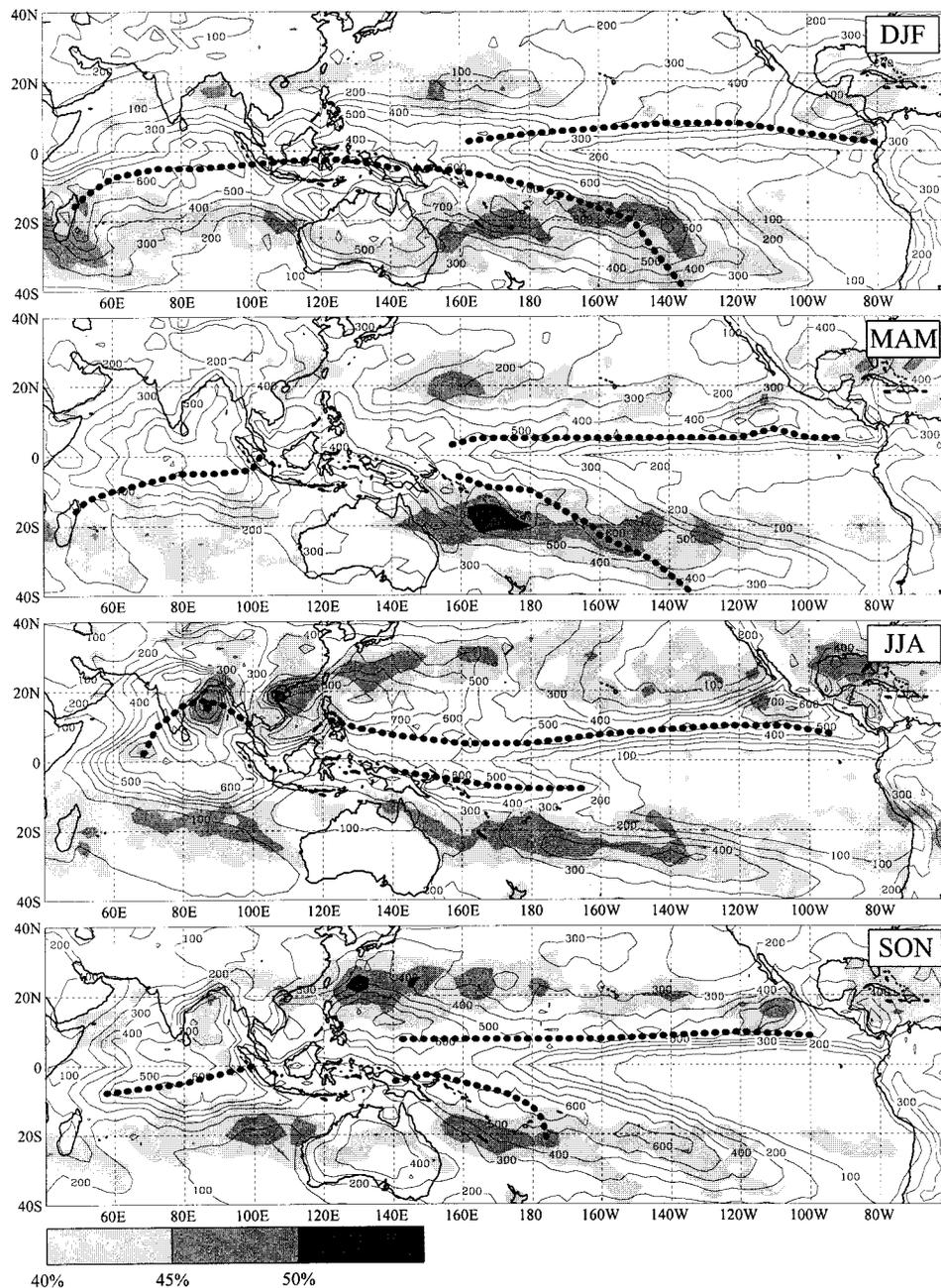
FIG. 5. Variance of 6–25-day bandpass-filtered OLR in W² m⁻⁴, for the seasons indicated. Shading represents the percent of the total variance (with the annual cycle of OLR removed) explained by the 6–25-day band. Dotted lines represent the axes of minimum OLR.

5. Interannual variability of ISO convective bands

Only a small number of papers has been written about the interannual variability of ISO convective bands, especially with regard to the 6–25-day band. The primary reason has been the lack of a sufficiently long homogeneous dataset. Papers that have focused on year-to-year changes in MJO convection include Holland (1986), Murakami et al. (1986), Lau and Chan (1988), Gutzler (1991),

and Anyamba and Weare (1995). The only paper that we are aware of that treats the interannual variability of the higher frequency ISO convective events is an internal one (Schrage and Vincent 1996) in which the 7–21-day band was examined. In that paper, however, the period of investigation encompassed only one ENSO cycle, and it did not explore changes in the NH Tropics. In this section of the paper, we will illustrate and discuss the interannual
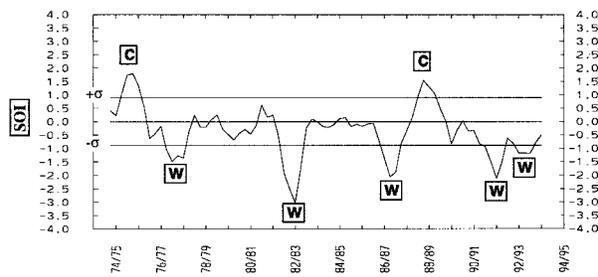
FIG. 6. Five-month running mean of the Southern Oscillation index. Thresholds for our definitions of El Niño and La Niña (i.e., ±1 standard deviation) are also plotted, as are the warm (W) and cold (C) events.

variability of OLR associated with ENSO events in both the MJO (25–70-day) and 6–25-day bands.

During the period of our investigation (1974–94), there were five El Niño and two La Niña events. Our selection of El Niño and La Niña periods is based on the SOI. A season was defined to be part of an El Niño (La Niña) event when its SOI value was greater than one standard deviation below (above) zero. Figure 6 shows a reproduction of the time series of SOI. The five El Niño events are 1977–78, 1982–83, 1986–87, 1991–92, and 1992–93, while the two La Niña events are 1975–76 and 1988–89. We realize that the 1992–93 period as well as most of 1994 are more commonly referred to as extensions of the 1991–92 El Niño (e.g., Bigg 1995); however, we decided to include the 1992–93 period as a separate event because it met our definition. We could not examine the second resurgence of the El Niño, which took place in the middle of 1994, because our OLR dataset ended in April of that year. We have opted to use the DJF season to represent all El Niño and La Niña events because this season showed the most consistent signal.

A composite map of the anomalous variance of filtered OLR, averaged over the five El Niño DJF seasons for each of our bands, is shown in Fig. 7. Also shown are some regions where averages were compiled for anomalous total and bandpass variances of OLR, which are discussed later. One of the more salient features in the variance patterns occurs near the equatorial central Pacific, east of 170°E, where maxima of positive anomalies occur in both bands. The patterns in Fig. 7 also show that the 6–25-day band makes an important positive contribution to the convective signal associated with ENSO variations along the diagonal axis of the SPCZ, whereas the 25–70-day band does not. This pattern is compatible with our results (Figs. 2, 4, and 5) that, as subtropical latitudes are approached, the contribution by the 6–25-day band becomes greater. The pattern is also compatible with the observation that the SPCZ is farther east and equatorward of its normal location in DJF during ENSO warm events (e.g., Vincent

1994). Finally, note that there are negative anomalies in both bands in the NH central Pacific centered at about 20°N, 160°W. More about this feature, which is stronger in the 6–25-day band, will be said below. There are other locations where large anomalies of the same sign coincide in the variance of both bands (e.g., negative anomalies over the Philippine Sea and positive anomalies centered near 20°S, 80°E). On the other hand, there are regions where the signs of anomalous variance in each band oppose one another (e.g., the eastern Indian Ocean).

To gain a better understanding of the ENSO variability associated with the 25–70- and 6–25-day bands, we now show their contributions to anomalous variance for each of our El Niño and La Niña events for a selection of regions. Anomalies of the total variance are also shown. The regions were shown in Fig. 7c, and bar graphs of anomalous variance are provided in Fig. 8. Because the Bay of Bengal showed a strong El Niño signal in SON, we have also included the graph of this region in Fig. 8.

Figure 8a shows results, which have been averaged over the equatorial eastern Indian Ocean. This region was selected because it contained opposing anomalies between the two bands in the El Niño composites (Fig. 7). It is seen that an out-of-phase relationship between the MJO and 6–25-day convection bands occurred during the first three El Niño events, with the MJO showing decreased convective variability. In four of the five El Niño events, the MJO shows decreased variability, while in the 6–25-day band increased variability was observed in four of five El Niños. This is an intriguing result for which we have no plausible explanation at the present time. Moreover, there is no consistent signal in Fig. 8a regarding the sign of anomalous total variance.

Proceeding eastward, the next region for which results are illustrated is northwestern Australia (Fig. 8b). This area contained peak values of anomalously low variance for the MJO band in the El Niño composite (Fig. 7a). This region also showed maximum variance in DJF for the 6–25-day band (Fig. 5). It is difficult to conclude any relationship between either band and the phase of ENSO, although three of the El Niño events show large negative anomalies in the MJO band. Our results can be compared to those of Drosdowsky (1996), who argued that no dominant spectral peak occurred from year to year on ISO timescales during the summer monsoon over northern Australia. We show both positive and negative anomalies in each band during DJF, thus our results support his argument. We can also compare our results to those of Evans and Allan (1992), who showed that tropical cyclone activity over northwestern Australia increased during the four El Niño events they sampled (the January–February months of 1966, 1973, 1983, and 1987). The last two of their events coincide with two
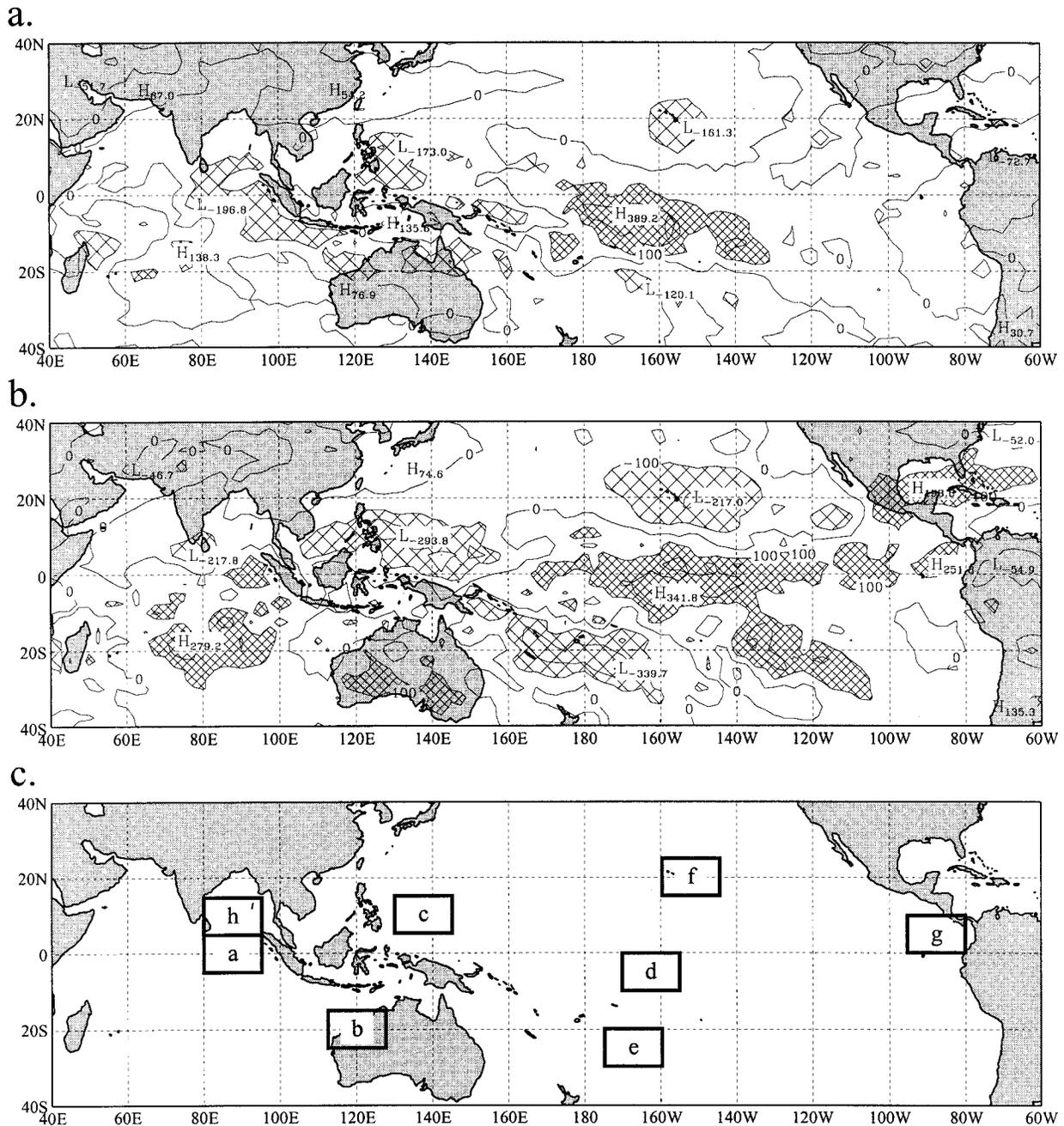
a.

b.

c.

FIG. 7. Composites of anomalous variance of OLR in the (a) 25–70-day and (b) 6–25-day band for five El Niño years (i.e., 1977–78, 1982–83, 1986–87, 1991–92, and 1992–93). (c) Domains used in Fig. 8.

of ours. If we assume that these cyclones fall within our 6–25-day band, Fig. 8b shows that our results agree with those of Evans and Allan in that our largest positive anomalies in this band occurred during the 1982–83 and 1986–87 El Niño events. In this context, however, our results do not show positive anomalies in the other three El Niños. Thus, one should be cautious about generalizing this result of Evans and Allan.

The next region for which results are shown is the NH tropical western Pacific, east of the Philippines (Fig. 8c). Figure 7 shows this as an area of anomalously low variance in both bands during El Niño events. In contrast to Figs. 8a and 8b, Fig. 8c reveals that El Niños persistently produce lower-than-normal variance in both ISO bands. Note further that in the three strongest El Niño events (i.e., 1982–83, 1986–87, and 1991–92, according to the SOI in Fig. 6), the anomalies in the 6–25-day band are greater than those in the MJO band.
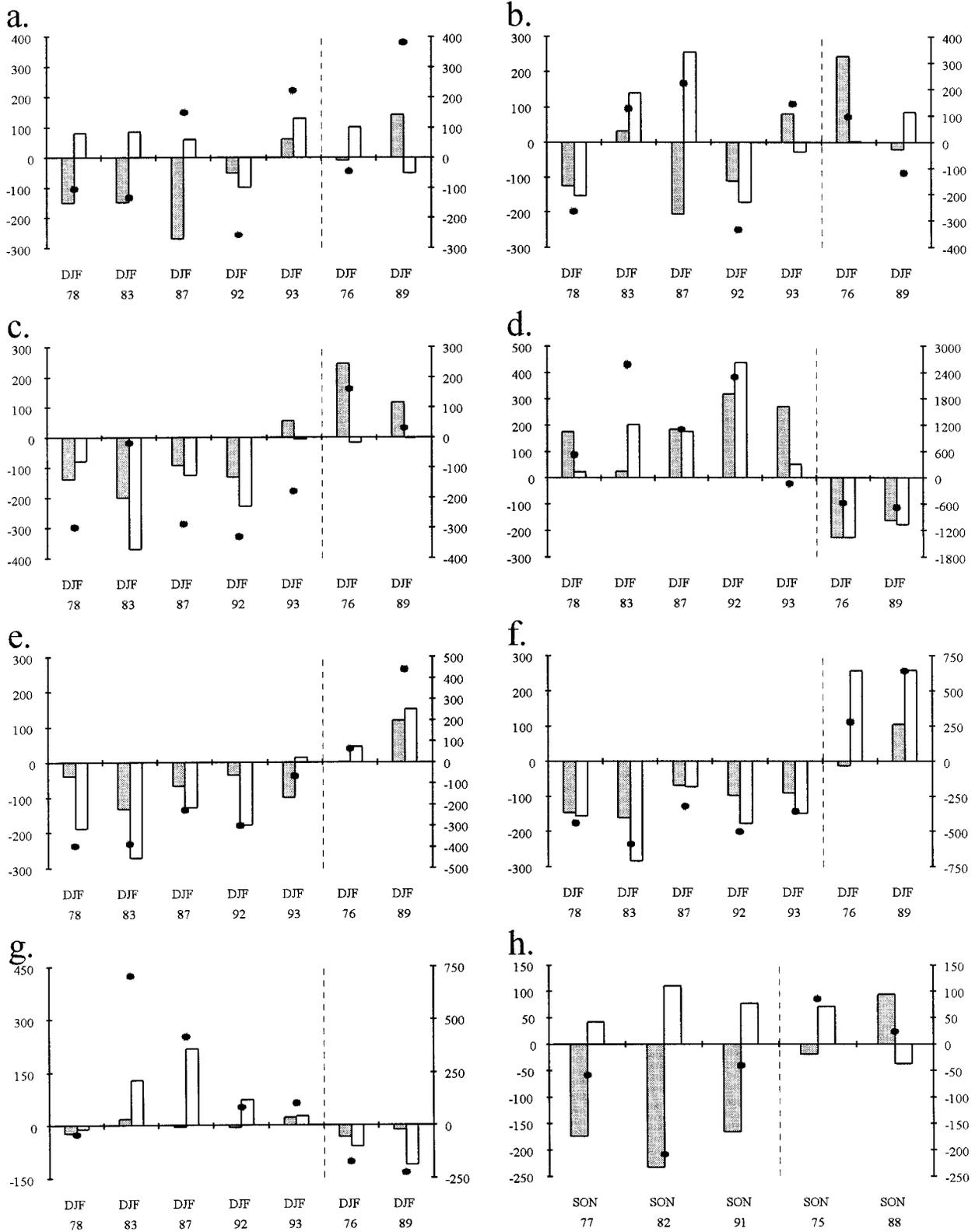
FIG. 8. Anomalous variance of (shaded) 25–70-day and (unshaded) 6–25-day bandpass-filtered OLR for five El Niño and two La Niña seasons, in W² m⁻⁴ on the left axis. Anomalies of total variance with the annual cycle of OLR removed) are plotted as solid dots in W² m⁻⁴ with respect to the right axis. El Niño (La Niña) seasons are plotted to the left (right) of the vertical dashed line. Domains for each panel are shown in Fig. 7c.
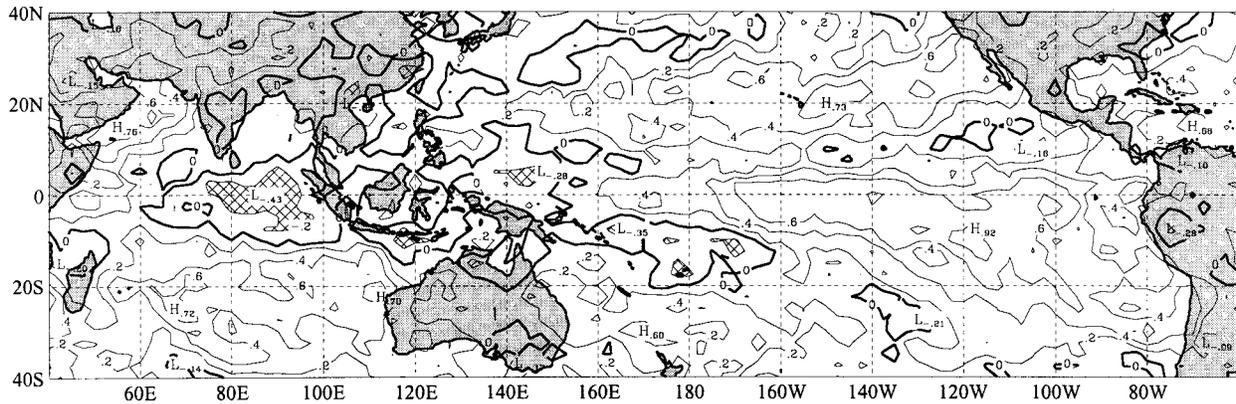
FIG. 9. Gridded correlation coefficients between anomalous variances in the 6–25-day and 25–70-day bands. Values below −0.20 are hatched, which is approximately the 95% confidence level for $n = 74$ independent observations. (The true threshold is −0.236.)

Also of importance is that, during the two La Niña periods, high positive anomalies occur in the MJO band, whereas there is no significant signal for the sign of anomalous variance in the 6–25-day band. Thus, the roles of the two bands appear to be well defined in this region and are consistent, especially for the MJO, with the expected eastward shift of convective activity during El Niño events. It is interesting to compare our results for the MJO band to those from Gutzler (1991). He found that the MJO signal in the low-level zonal winds was enhanced during El Niño events between 140°E and 170°W, but not west of 140°E. Our results in Fig. 8c show that in the four strongest El Niños, MJO convective variability is suppressed, suggesting that our region c, which straddles 140°E, is representative of convective processes to the west of 140°E.

Over the central Pacific Ocean, there are three regions displayed, one near the equator and the other two at subtropical latitudes, with one in each hemisphere. The near-equatorial region (Fig. 8d) shows a clear picture of positive anomalies of variance in both bands during the El Niño events and negative anomalies during La Niña events, although the relative differences in enhanced convective variability between the two bands varies from one El Niño to the next. Note, in particular, that the weakest signal in the MJO band occurs in the strongest El Niño, 1982–83. Our results for this event can be compared to those from Lau and Chan (1988) and Anyamba and Weare (1995). Lau and Chan used EOF analyses and time series to show that the 1982–83 El Niño contained an overall pattern for the MJO band, which was quite weak. Our results certainly support their finding. On the other hand, the remaining four El Niños in our sample show large positive anomalies in the MJO band, suggesting that Lau and Chan's conclusion should not be generalized. Anyamba and Weare (1995) found that the eastward propagation of the MJO in the 1982–83 El Niño was suppressed compared to

other ENSO events. This would indicate that the relative strength of MJO convection over the central Pacific would not be as strong during this El Niño, a characteristic seen in our results.

Next, we examine the results for the two subtropical locations, north and south of region d. These regions, which are close to the long-term climatological position of the SPCZ (Fig. 8e) and to Hawaii (Fig. 8f), show results that are essentially opposite to those in Fig. 8d. All five El Niños over both regions contain relatively strong negative anomalies in each band, whereas positive anomalies dominate in the two La Niña periods.

Several additional points are worth noting with regard to the graphs in Figs. 8c–f. First, in Figs. 8e and 8f, the magnitude of both positive and negative anomalies is generally much greater in the 6–25-day band than it is in the 25–70-day band. This is not surprising, since higher-frequency ISOs tend to become more important as one progresses away from the equator (see Fig. 5). Second, the results for the South Pacific region are not unexpected, since the SPCZ is known to be much farther east and north of its climatological position during El Niño events. Third, there appears to be a definite out-of-phase relationship between the ISO bands in Fig. 8e and Fig. 8f and those in Fig. 8d, suggesting that there is a connection in the meridional plane between the tropical and subtropical convective patterns, regardless of whether a warm or cold event is occurring. It is speculated that the pattern of OLR anomaly teleconnections, which is excited when strong MJO events arrive at the dateline and which extends from the equatorial central Pacific northeastward toward Baja California and then southeastward toward the northern tip of South America (see Knutson and Weickmann 1987, their Fig. 9, as well as Rui and Wang 1990, their Fig. 3f), is shifted eastward during El Niño events. In normal or La Niña years, this wave train should cause enhanced convection over the subtropical central Pacific (Kiladis

et al. 1994; Meehl et al. 1996) on the 6–25-day bands during DJF. Our results support this pattern. Lastly, there also appears to be an out-of-phase relation in the Tropics between the ISOs over the northwestern Pacific (Fig. 8c) and those over the central Pacific (Fig. 8d).

Figure 8g shows the graphical results for the NH tropical eastern Pacific region. This area was chosen because it contains a peak in the positive anomaly of the 6–25-day band in the El Niño composite (Fig. 7). This region is also situated near the ITCZ, although the convergence zone is not as strong in DJF as it is in the other three seasons. The graphs clearly show that the 6–25-day band dominates over the MJO band and that positive anomalies occur in the former band in all but the 1977–78 El Niño, while negative anomalies occur during the two La Niña periods.

The last set of graphs shown is for the Bay of Bengal region in the SON season (Fig. 8h). The only three El Niño events that met our SOI criteria in SON were those that occurred in 1977, 1982, and 1991. It is seen that the convection anomalies associated with the two bands oppose each other in all of the El Niño and La Niña events shown, with the magnitude of the MJO anomaly being greater than its opposing 6–25-day band during the three El Niño events. Moreover, during El Niño events, the MJO band shows negative anomalies. This anticorrelation between the bands, and the tendency of the MJO band to contain suppressed convective variability during ENSO warm cases, was also found in DJF for the region adjacent and equatorward of the Bay of Bengal (Fig. 8a). This suggests that the same processes, shifted northward in accord with the annual cycle of the monsoon, may be responsible for the observed anomalies.

6. Correlations between the two bands

The correlation between the anomalous signal strengths in the 25–70- and 6–25-day bands is presented in Fig. 9. At subtropical latitudes (e.g., Arabian Sea, central North Pacific, southern Indian Ocean, and eastern South Pacific), it is seen that rather high positive correlations between the two bands are prominent. This, no doubt, is due to the fact that convection occurs infrequently at these latitudes, and any convective anomaly adds power to both spectral bands. Near the equator, therefore, is where the correlation patterns are more meaningful. Figure 9 shows an interesting distribution of correlations stretching along the equator from the central Indian Ocean, eastward to the eastern Pacific. Over the Indian Ocean, a region of negative values exists, while over the Maritime Continent, near-zero values are prominent. Finally, over the main body of the Pacific Ocean, there is an elongated region of positive correlations. Since the main source of 25–70-day variability should be equatorially trapped MJO events, this chang-

ing feedback between the two temporal scales as one proceeds eastward warrants an explanation.

The anticorrelation in the Indian Ocean was found to be a rather robust phenomenon. Time series of anomalous variance in both bands are given for each season for a box centered on this feature (Fig. 10). The anticorrelation of the bands is apparent in all seasons except JJA, at which time this domain experiences relatively little year-to-year variability in the MJO band (Fig. 10c). For the entire 20-yr period, this anticorrelation was significant at the 95% level over a wide area of the east Indian Ocean (Fig. 9). A plausible explanation of this phenomenon is related to the combined effect of two factors. First, Fig. 10 suggests that the (available) convective energy over the Indian Ocean is frequently released by higher-frequency disturbances during episodes of a weak and irregular MJO signal. Second, from an inspection of the time series of OLR in the eastern Indian Ocean (not shown) for a period (October 1987–April 1988), which contained a highly active MJO band (identified by the arrow in Fig. 10a), it was evident to us that the "dry phase" of the MJO was characterized by the total absence of deep convection.

In sharp contrast to the events over the Indian Ocean, the inactive phase of the MJO over the western Pacific warm pool experienced frequent convective events on timescales shorter than the MJO (not shown). This observation, and the stronger seasonality over the western Pacific warm pool, results in the zero correlation evident in Fig. 9. The positively correlated results for the equatorial central Pacific can be interpreted as the difference between El Niño and La Niña convective patterns. Gutzler (1991) observed the same phenomena in the low-level winds at Canton Island (3°S, 172°W). An examination of our time series (not shown) clearly demonstrated that neither band exhibits much power in this region until the onset of an ENSO warm event, at which time the shifting convective and circulation regimes result in highly anomalous power at all frequencies.

7. Discussion and concluding remarks

The present paper was aimed at performing a comprehensive study into the behavior of higher- (6–25-day) and lower- (25–70-day or MJO) frequency bands of tropical intraseasonal convective oscillations. Due to the length of our dataset (1974–94), we were able to obtain results with a considerable degree of detail, especially on ENSO timescales. Emphasis was given to the interannual variability of both bands, but particular attention was devoted to the 6–25-day band, which has not appeared frequently in the literature.

The climatology of high- and low-frequency ISOs revealed that these phenomena occurred over broad regions of the Tropics and subtropics. In a general sense, the zones with the strongest intraseasonal signals tended to align with well-known convective domains such as the ITCZ and SPCZ. A close examination of our results,
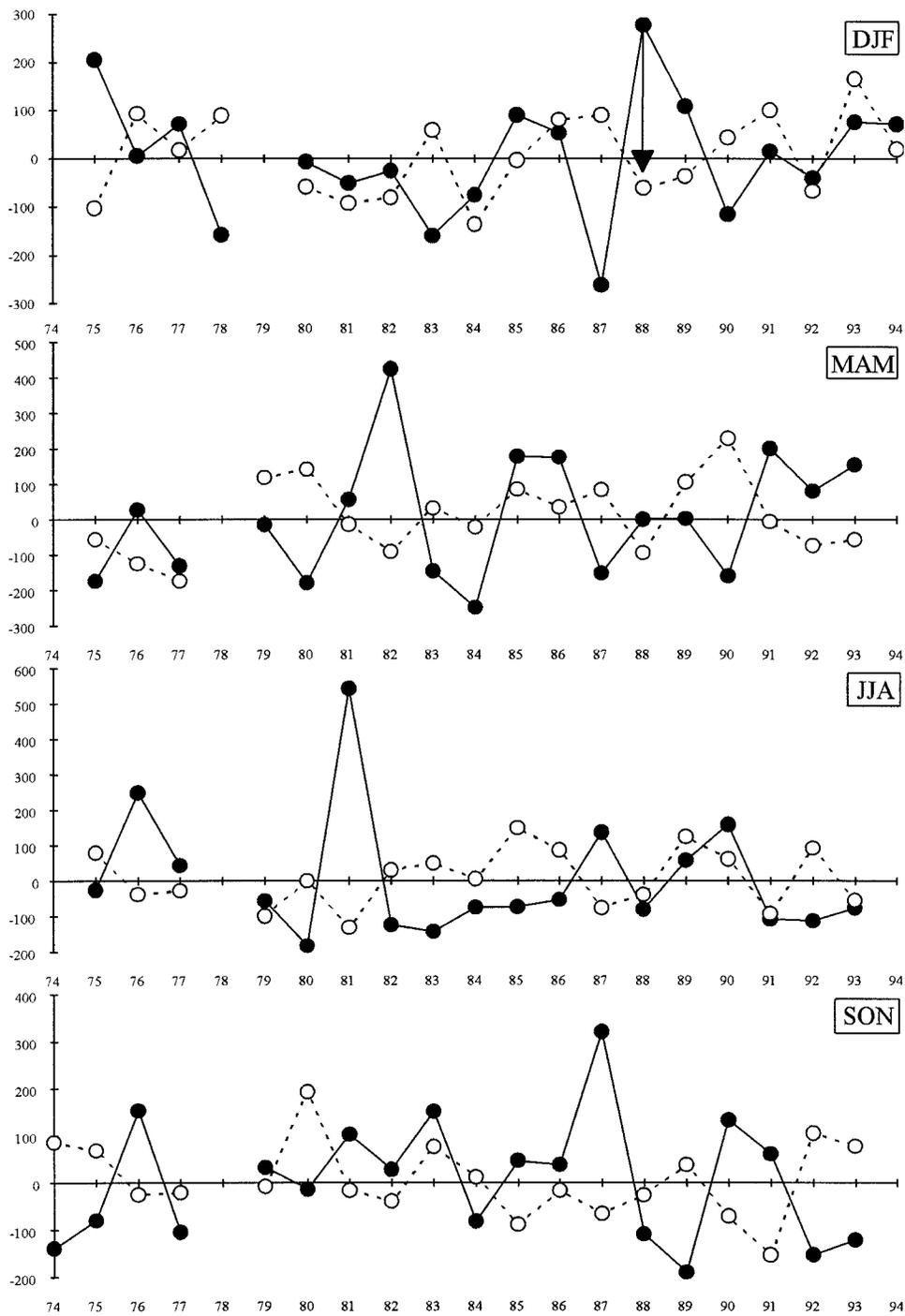
FIG. 10. Time series of seasonal anomalous variance in the 25–70-day (solid dots) and 6–25-day (open circles) bands for a 10° × 15° box centered at 0°, 90°E. See text for meaning of the arrow in top panel.

however, revealed that differences frequently occurred between the two spectral bands. Some important examples were 1) in DJF, the activity in the MJO band was concentrated in the eastern Indian Ocean, while strong 6–25-day convective variability extended all the way across the Indian Ocean from the east coast of

Madagascar to the west of Sumatra; 2) the 6–25-day OLR variance attained its all-season maximum over the northern Bay of Bengal in JJA, whereas the seasonal maximum within the MJO band was found 15° to the south; and 3) in the SH western Pacific, the axis of

maximum 6–25-day variability was displaced 7°–10° poleward of the 25–70-day and ITCZ axes in DJF.

In each of these cases, the higher-frequency intraseasonal convective perturbations were associated with independent phenomena. With regard to the first example, Jury et al. (1991) and Jury and Pathack (1991) found that easterly waves over the southwestern Indian Ocean made an important contribution to periods that fall within our 6–25-day band. Concerning point 2, Nitta et al. (1985), Hartmann and Michelsen (1989), and Lau and Lau (1990) found considerable power on 5–8-day timescales associated with westward-propagating monsoon depressions over the northern Bay of Bengal. Finally, with regard to the last point, Ko and Vincent (1995), Schrage and Vincent (1996), and Vincent et al. (1997) found that tropical–extratropical interactions played an important role in the SH 6–25-day band.

An interesting relation between the bands existed over the eastern Indian Ocean. During seasons when the MJO signal was weaker than normal, the 6–25-day band demonstrated anomalous power. Likewise, the 6–25-day band frequently contained less power during times that were characterized by an anomalously strong and regular MJO signal. This anticorrelation was statistically significant only in the eastern Indian Ocean and occurred regardless of the phase of ENSO. We speculate that two factors, in combination, might be responsible. First, in the off-equatorial SH eastern Indian Ocean, 6–25-day convective variability is quite large, especially during the summer season when tropical wave and cyclone activity are at a maximum. Jury et al. (1991) and Jury and Pathack (1991) found that this activity caused spectral peaks within the range of 1–4 weeks. Second, time series of both 6–25- and 25–70-day anomalous variance revealed that the dry phase of an active MJO episode was characterized by the absence of deep convection. Bladé and Hartmann (1993) found a drying of the lower troposphere at Singapore after the passage of MJO events, which, together with their modeling results, led them to speculate that MJO events "discharge" available convective energy, which "recharge" over a period of a few weeks (i.e., within the 6–25-day band). In contrast to the Indian Ocean, the 6–25-day convective variability was strong over the western Pacific warm pool (e.g., the region east-southeast of New Guinea) despite the presence of passing MJO events. Since SSTs in the warm pool are about 1°C higher than over the eastern Indian Ocean, and the columnar water vapor content exceeds that of the Indian Ocean by about 10%–20% (Stephens et al. 1994, their Fig. 3), one might speculate that only the warm pool SSTs are high enough to support continuous convective activity in all frequency bands. Clearly, this feature warrants further investigation.

One of the fundamental goals of this study was to document the effects of the ENSO cycle on intraseasonal variability. Compositing the DJF variance anomalies in each spectral band with respect to El Niño events re-vealed a pattern of increased (decreased) convective variability in the central Pacific (western Pacific, east of the Philippines) in both intraseasonal bands. Composited OLR anomalies for the same El Niño seasons were shown in Fink and Speth (1998). Their results lead us to conclude that the anomalies in both bands are due to the general pattern of the eastward displaced Walker circulation at those times; that is, convection is generally enhanced (decreased) over the central Pacific (the Philippine Sea). During the two La Niña cases, we found that both bands also exhibited coherent anomalies, but, in accord with the anomalous westward position of the Pacific Walker cell, anomalies were of opposite sign. Our findings are consistent with those of Gutzler (1991) in that he found the best correlation between the SOI and the intraseasonal variance in the low-level wind at his easternmost station, Canton Island (3°S, 172°W). However, he was not able to identify the aforementioned anomaly dipole between the central Pacific and the Philippine Sea, since he had no data in the latter region.

Another intriguing feature in our results, which presumably is related to tropical–extratropical interactions, was the meridional anomaly pattern found over the central Pacific in DJF. While the variance in both bands increased (decreased) significantly in the equatorial central Pacific, it decreased (increased) in the subtropical latitudes of both hemispheres (regions e and f in Fig. 7c). At least for the Hawaiian box, the OLR fails to be a reliable proxy of deep moist convection due to the frequent occurrence of upper-level cirrus clouds in connection with the subtropical jet streams. However, this correlation is consistent with the notion of an ENSO-related eastward shift of teleconnection patterns that, in the climatological mean, emanate from the tropical central Pacific into the subtropical latitudes of either hemisphere (e.g., Knutson and Weickmann 1987; Rui and Wang 1990; Kiladis et al. 1994; Meehl et al. 1996).

The ENSO signal in each band was found to be inconclusive over the eastern Indian Ocean and northwestern Australia. While the first three El Niños of 1977–78, 1982–83, and 1986–87, showed uniform anomalies over the Indian Ocean, Anyamba and Weare (1995) could not find a coherent El Niño signal in the oscillations' large-scale spatial characteristics for the same cases. During the 1991–92 and 1992–93 warm cases, however, we found that the anomalies of the bands were weak and not consistent with the earlier cases. Therefore, our results also do not support the view that a uniform response of both bands to El Niño conditions existed over the Indian Ocean. The lack of significant correlation for the northwestern Australian region is in accord with the findings of McBride and Nicholls (1983) and Drosdowsky and Williams (1991). They found that the Australian rainfall was solely correlated with the SOI in the transition season (SON), but this correlation broke down during the peak of the monsoon season. It is interesting to note, however, that during two of our El Niños (1982–83 and 1986–87), which were part of

the four El Niños studied by Evans and Allen (1992), the 6–25-day band showed positive anomalies. While this would corroborate their results (see discussion in section 5), two other El Niños outside their sample showed negative anomalies. These differences point to a sampling problem and, evidently, a larger sample of El Niño events is required to answer this important question.

Clearly, our results need to be substantiated by studies of variables, which are related to the convective bands documented here. Reliable observations of precipitable water (W) need to be examined, and our investigation should be complemented by studies of the relationships between the convective signals of ISOs and circulation parameters, such as velocity potential, low- and upper-level winds, vertical velocity, and vorticity. The recent availability of reanalysis datasets offers an excellent opportunity to perform some of these studies. Furthermore, as stated in section 2, several convective phenomena contribute to the power in both bands, but their regionally varying contributions are important and need to be examined in detail. In this regard, our study suggests that regional case studies should be pursued to substantiate the underlying physical causes, which explain the different behavior of the bands, especially on ENSO timescales.

REFERENCES

Anyamba, E. K., and B. C. Weare, 1995: Temporal variability of the 40–50 day oscillation in tropical convection. *Int. J. Climatol.,* **15,** 379–402.

Bigg, G. R., 1995: The El Niño event of 1991–94. *Weather,* **50,** 117–124.

Bladé, I., and D. L. Hartmann, 1993: Tropical intraseasonal oscillations in a simple nonlinear model. *J. Atmos. Sci.,* **50,** 2922–2939.

Drosdowski, W., 1996: Variability of the Australian summer monsoon at Darwin: 1957–1992. *J. Climate,* **9,** 85–96.

——, and M. Williams, 1991: The southern oscillation in the Australian region. Part I: Anomalies at the extremes of the oscillation. *J. Climate,* **4,** 619–638.

Evans, J. L., and R. J. Allan, 1992: El Niño Southern Oscillation modification to the structure of the monsoon and tropical cyclone activity in the Australasian region. *Int. J. Climatol.,* **12,** 611–623.

Fink, A., and P. Speth, 1998: Some potential forcing mechanisms of the year-to-year variability of the tropical convection and its intraseasonal (25–70 day) variability. *Int. J. Climatol.,* in press.

Frank, W. M., 1987: Tropical cyclone formation. *A Global View of Tropical Cyclones,* R. L. Elsberry, Ed., University of Chicago Press, 53–90.

Fuell, K., 1997: The annual cycle and interannual variability of synoptic (3–7 day) and intraseasonal (7–25 day) convective activity over the tropical eastern Pacific. M.S. thesis, Dept. of Earth and Atmos. Sci., Purdue University, 78 pp. [Available from Dept. of Earth and Atmos. Sci., Purdue University, West Lafayette, Indiana 47907.]

Gruber, A., and F. Krueger, 1984: The status of the NOAA outgoing longwave radiation data set. *Bull. Amer. Meteor. Soc.,* **65,** 958–962.

Gutzler, D. S., 1991: Interannual fluctuations of intraseasonal variance of near-equatorial zonal winds. *J. Geophys. Res.,* **96,** 3173–3185.

Hartmann, D. L., and M. L. Michelsen, 1989: Intraseasonal periodicities in Indian rainfall. *J. Atmos. Sci.,* **46,** 2838–2862.

——, ——, and S. A. Klein, 1992: Seasonal variations of tropical intraseasonal oscillations: A 20–25 day oscillation in the western Pacific. *J. Atmos. Sci.,* **49,** 1277–1289.

Hendon, H. H., and B. Liebmann, 1990: A composite study of onset of the Australian summer monsoon. *J. Atmos. Sci.,* **47,** 2227–2240.

Holland, G. J., 1986: Internannual variability of the Australian summer monsoon at Darwin: 1952/82. *Mon. Wea. Rev.,* **114,** 594–604.

Jury, M. R., and B. Pathack, 1991: A study of climate and weather variability over the tropical southwest Indian Ocean. *Meteor. Atmos. Phys.,* **47,** 37–48.

——, ——, G. Campbell, B. Wang, and W. Landman, 1991: Transient convective waves in the tropical SW Indian Ocean. *Meteor. Atmos. Phys.,* **47,** 27–36.

Kiladis, G. N., and K. M. Weickmann, 1992a: Circulation anomalies associated with tropical convection during northern winter. *Mon. Wea. Rev.,* **120,** 1900–1923.

——, and ——, 1992b: Extratropical forcing of tropical convection during northern winter. *Mon. Wea. Rev.,* **120,** 1924–1938.

——, G. A. Meehl, and K. M. Weickmann, 1994: Large-scale circulation associated with westerly wind bursts and deep convection over the western equatorial Pacific. *J. Geophys. Res.,* **99,** 18 527–18 544.

Knutson, T. R., and K. M. Weickmann, 1987: 30–60 day atmospheric oscillation: Composite life cycles of convection and circulation anomalies. *Mon. Wea. Rev.,* **115,** 1407–1436.

——, ——, and J. E. Kutzbach, 1986: Global-scale intraseasonal oscillations of outgoing longwave radiation and 250 mb zonal wind during northern hemisphere summer. *Mon. Wea. Rev.,* **114,** 605–623.

Ko, K.-C., and D. G. Vincent, 1995: A composite study of the quasi-periodic subtropical wind maxima over the South Pacific during November 1984–April 1985. *J. Climate,* **8,** 579–588.

——, and ——, 1996: Behavior of one to two week summertime subtropical wind maxima over the South Pacific during an ENSO cycle. *J. Climate,* **9,** 5–16.

Lau, K.-H., and N.-C. Lau, 1990: Observed structure and propagation characteristics of tropical summertime synoptic scale disturbances. *Mon. Wea. Rev.,* **118,** 1888–1913.

Lau, K.-M., and P. H. Chan, 1985: Aspects of the 40–50 day oscil-

lation during northern winter as inferred from outgoing longwave radiation. *Mon. Wea. Rev.,* **113,** 1889–1909.

——, and ——, 1988: Intraseasonal and interannual variations of tropical convection: A possible link between the 40–50 day oscillation and ENSO. *J. Atmos. Sci.,* **45,** 506–521.

——, ——, C. H. Sui, and T. Nakazawa, 1989: Dynamics of super cloud clusters, westerly wind bursts, 30–60 day oscillations and ENSO: A unified view. *J. Meteor. Soc. Japan,* **67,** 205–219.

——, T. Nakazawa, and C. H. Cui, 1991: Observations of cloud cluster hierarchies over the tropical western Pacific. *J. Geophys. Res.,* **96,** 3197–3208.

Madden, R. A., and P. R. Julian, 1971: Detection of a 40–50 day oscillation in the zonal wind in the tropical Pacific. *J. Atmos. Sci.,* **28,** 702–708.

——, and ——, 1972: Description of global-scale circulation cells in the tropics with a 40–50-day period. *J. Atmos. Sci.,* **29,** 1109–1123.

——, and ——, 1994: Observation of the 40–50-day tropical oscillation—A review. *Mon. Wea. Rev.,* **122,** 813–837.

McBride, J. L., and N. Nicholls, 1983: Seasonal relationships between Australian rainfall and the southern oscillation. *Mon. Wea. Rev.,* **111,** 1998–2004.

Meehl, G. A., 1987: The annual cycle and interannual variability in the tropical Pacific and Indian Ocean regions. *Mon. Wea. Rev.,* **115,** 27–50.

——, G. N. Kiladis, K. M. Weickmann, M. Wheeler, D. S. Gutzler, and G. P. Compo, 1996: Modulation of equatorial subseasonal convective episodes by tropical-extratropical interaction in the Indian and Pacific Ocean regions. *J. Geophys, Res.,* **101,** 15 033–15 049.

Murakami, M., 1979: Large-scale aspects of deep convective activity over the GATE area. *Mon. Wea. Rev.,* **107,** 994–1038.

Murakami, T., 1980: Temporal variations of satellite-observed outgoing longwave radiation over the winter monsoon region. Part I: Long-period (15–30 day) oscillations. *Mon. Wea. Rev.,* **108,** 408–426.

——, and W. L. Sumathipala, 1989: Westerly bursts during the 1982/83 ENSO. *J. Climate,* **2,** 71–85.

——, L.-X. Chen, A. Xi, and M. L. Shrestha, 1986: Eastward propagation of 30–60 day perturbations as revealed from outgoing longwave radiation data. *J. Atmos. Sci.,* **43,** 961–971.

Nakazawa, T., 1988: Tropical super cloud clusters within intraseasonal variations over the western pacific. *J. Meteor. Soc. Japan,* **66,** 823–839.

——, and Y. Takayabu, 1985: Global analyses of the lower tropospheric disturbances in the tropics during the northern summer of the FGGE year. Part II: Regional characteristics of the disturbances. *Pure Appl. Geophys.,* **123,** 272–292.

Nitta, T., Y. Nakagomi, Y. Suzuki, N. Hasegawa, and A. Kadokura, 1985: Global analysis of the lower tropospheric disturbances in the tropics during the northern summer of the FGGE year. Part II: Global features of the disturbances. *J. Meteor. Soc. Japan,* **63,** 1–18.

Rui, H., and B. Wang, 1990: Development characteristics and dynamic structure of tropical intraseasonal convection anomalies. *J. Atmos. Sci.,* **47,** 357–379.

Schnadt, C., 1997: 6–25-day westward-propagating convective disturbances over the Northern Hemisphere tropical West Pacific: A mechanism for tropical-extratropical interaction. M.S. thesis, Institute for Geophysics and Meteorology, University of Cologne, 133 pp. [Available from Institute for Geophysics and Meteorology, University of Cologne, Albertus-Magnus-Platz/Kerpener Strasse, D-50923 Cologne, Germany.]

Schrage, J. M., and D. G. Vincent, 1996: Tropical convection on 7–21-day timescales over the western Pacific. *J. Climate,* **9,** 587–607.

Stearns, S. D., and D. R. Hush, 1990: *Digital Signal Analysis.* 2d ed. Prentice-Hall, 440 pp.

Stephens, G. L., D. L. Jackson, and J. J. Bates, 1994: A comparison of SSM/I and TOVS column water vapor data over global oceans. *Meteor. Atmos. Phys.,* **54,** 183–201.

Sui, C.-H., and K.-M. Lau, 1992: Multiscale phenomena in the tropical atmosphere over the western Pacific. *Mon. Wea. Rev.,* **120,** 407–430.

Vincent, D. G., 1994: The South Pacific convergence zone (SPCZ): A review. *Mon. Wea. Rev.,* **122,** 1949–1970.

——, and J. Schrage, 1995: *Climatology of the TOGA-COARE and Adjacent Regions (1985–1990): Thermodynamic and Moistures Variables (Volume 2).* Purdue University, 104 pages.

——, T. Sperling, A. Fink, S. Zube, and P. Speth, 1991: Intraseasonal oscillation of convective activity in the tropical southern hemisphere: May 1984–April 1986. *J. Climate,* **4,** 40–53.

——, K.-C. Ko, and J. M. Schrage, 1997: Subtropical jet streaks over the South Pacific. *Mon. Wea. Rev.,* **125,** 438–447.

Wang, B., and H. Rui, 1990: Synoptic climatology of transient tropical intraseasonal convection anomalies. *Meteor. Atmos. Phys.,* **44,** 43–61.

Weickmann, K. M., G. R. Lussky, and J. E. Kutzbach, 1985: Intraseasonal (30–60 day) fluctuations of outgoing longwave radiation and 250 mb streamfunction during northern winter. *Mon. Wea. Rev.,* **113,** 940–961.

Zhu, B., and B. Wang, 1993: The 30–60 day convection seesaw between the tropical Indian Ocean and the western Pacific Oceans. *J. Atmos. Sci.,* **50,** 184–199.